Development of a total variation diminishing (TVD) Sea ice transport scheme and its application in in an ocean (SCHISM v5.11) and sea ice (Icepack v1.3.4) coupled model on unstructured grids

5   Qian Wang[1,2], ~~Yang Zhang[2],~~ Fei Chai[1,2,3], ~~Yang Zhang[2],~~ Y. Joseph Zhang[4], Lorenzo Zampieri~~Zamperi~~[5]

1. School of Oceanography, Shanghai Jiao Tong University, Shanghai, China
2. State Key Laboratory of Satellite Ocean Environment Dynamics, Second Institute of Oceanography, Ministry of Natural Resources, Hangzhou, China
10   3. State Key Laboratory of Marine Environmental Science, Xiamen University, Xiamen, China
4. Virginia Institute of Marine Science, Gloucester Point, VA, USA
5. Climate Simulations and Predictions Division, Centro Euro-Mediterraneo sui Cambiamenti Climatici (CMCC), Bologna, Italy

Correspondence to: Fei Chai (fchai@sio.org.cn) Yang Zhang (yzhang@sio.org.cn)

15   **Abstract.**   As the demand for increased resolution and complexity in unstructured sea ice models is growing, a more advanced sea ice transport scheme is needed. In this study, we couple the Semi-implicit Cross-scale Hydro-science Integrated System Model (SCHISM) with Icepack, the column physics package of the sea ice model CICE; a key step is to implement a total variation diminishing (TVD) transport scheme for the multi-class sea ice module in the coupled model. Compared with the second-order upwind scheme and the Finite Element Flux Corrected Transport scheme (FEM-FCT)~~a central difference scheme~~, the TVD transport scheme is found to have better performance for both idealized and realistic cases, and meets the requirements for conservation, accuracy, efficiency (even with very high resolution), and strict monotonicity. The new coupled model outperforms the existing single-class ice model of SCHISM in the case of the Lake Superior. ~~for~~For the Arctic Ocean case, it successfully reproduces the long-term changes in the sea ice extent, the sea ice boundary, ~~and~~ concentration observation from ~~the~~ satellites and thickness from in situ measurement.

1 Introduction

The dramatic~~ally~~ decrease in the Arctic ~~s~~Sea ice in recent decades attributable to global warming~~due to global warming~~ has a major impact on local and global climate (IPCC, 2019). In order to understand

30   the changes in the physical and biogeochemical processes occurring in the Arctic Ocean, numerical models have become an important tool and they have been significantly improved in the past few decades. The sea ice, as a highly complex material (Hunke et al., 2020), received special attention. Consequently, sea ice models have evolved, ~~now~~ offering better representation of the sophisticated

physical processes ~~involved~~and the sea ice models have become more sophisticated in representing realistic physics. At present, an advanced sea ice model, the Los Alamos sea ice model (CICE~~,~~. Hunke

35

et al., 2015), including a stand-alone column physics package Icepack (Hunke et al., 2020), has incorporated multi-class thermodynamics, such as the Bitz and Lipscomb (1999; BL99) thermodynamics formulation for constant salinity profiles, the mushy layer thermodynamics formulation for evolving salinity (Turner et al. 2013), and the sea ice ridging processes (Lipscomb et

40

al.~~Hunke~~, 20_07_~~10~~). Many structured-grid models have been coupled with Icepack or CICE directly or via couplers, e.g., the Community Earth System Model (CESM~~,~~. Hurrell et al.,2013) and the HYbrid Coordinate Ocean Model (HYCOM); others have partially incorporated and adapted CICE subroutines in their own ice module, e.g., the Sea Ice modelling Integrated Initiative (SI^3) of the Nucleus for European Modelling of the Ocean (NEMO, and NEMO can also couple with CICE or The Louvain-La-

45

Neuve sea ice model, LIM3, ~~Gurvan~~ Madec et al., 2022), and The Thermodynamic Sea Ice Package (THSICE) of the Massachusetts Institute of Technology General Circulation Model (MITgcm~~,~~. Adcroft ~~Campin~~ et al., 2023). For the unstructured-grid (UG) models, Gao et al. (2011) have incorporated the Unstructured-Grid CICE (UG-CICE) into the unstructured-grid Finite Volume Community Ocean Model (FVCOM, Chen et al., 2012). Some other unstructured-grid models have

50

incorporated Icepack directly, e.g., the Finite-volumE Sea ice-Ocean Model version 2 (FESOM2, Zampieri et al., 2021~~Danilov et al., 2017~~) and the Model for Prediction Across Scales (MPAS-Seaice, Turner et al., 2022). ~~Note that when Icepack is incorporated into another model, the latter must also implement its own dynamic solver for momentum and transport.~~ UG-CICE and FESOM2 utilize triangular mesh grids, whereas MPAS-Seaice employs a Voronoi dual graph.~~UG-CICE and FESOM2~~

55

~~use triangular mesh grids while MPAS-Seaice uses Voronoi dual graph.~~ UG-CICE is based on ~~uses~~ a finite-volume formulation, the sea ice component allows for five ice categories, four layers of ice and one layer of snow. The remaining models permit user specification of the number of ice categories.~~The other models allow users to specify the number of categories.~~ UG-CICE can produce good results on the seasonal variability of the sea ice in the Arctic Ocean (Gao et al., 2011). FESOM2, having

60

implemented Icepack comprehensively, demonstrates that additional complexity in model formulations can enhance simulation accuracy~~FESOM2 has implemented Icepack in its entirety and found that more complex model formulations lead to better results~~ (Zampieri et al., 2021). MPAS-Seaice can be viewed as the unstructured version of CICE, and thus shares sophisticated thermodynamics and

biogeochemistry with CICE, including BL99 and mushy layer, and is the current sea-ice component of the Energy Exascale Earth System Model (E3SM, Turner et al., 2022). A summary of these sea-ice models is given in Table 1.

Model	Ice model	Grid	Thermodynamic	Transport solver	Coupling method
CESM	CICE	Structured	BL99 Mushy Layer	Incremental remapping scheme/ Upwind scheme	Coupler
NEMO	CICE, LIM3, SI[3]	Structured	Mushy Layer	Prather scheme/ ULTIMATE-MACHO scheme (SI[3])	Direct (with SI[3])
HYCOM	CICE	Structured	BL99 Mushy Layer	Incremental remapping scheme/ Upwind scheme	Coupler
MITgcm	THSICE	Structured	Two layers of ice and one layer of snow	2nd-order flux limited scheme	Direct
E3SM	MPAS-Seaice	Unstructured	BL99 Mushy Layer	Incremental remapping scheme/ Upwind scheme	Coupler
UG-CICE	CICE	Unstructured	Four layers of ice and one layer of snow	Second order upwind scheme	Direct
FESOM2	ICEPACK	Unstructured	BL99 Mushy Layer	FEM-FCT	Direct

Table 1. Comparison of several sea ice models

SCHISM is a derivative product built from the original Semi-implicit Eulerian–Lagrangian Finite Element (SELFE, v3.1dc; Zhang and Baptista 2008) with multiple enhancements, including the seamless cross-scale capability from creek to ocean, a mass conservative, monotone, higher-order transport solver TVD[2] (implicit TVD in the vertical and explicit TVD in the horizontal, Zhang et al., 2016). SCHISM has been applied to study the Great Lakes ice formation process and obtained reasonable results in very high resolution (Zhang et al., 2023), using a single-class ice/snow module borrowed from FESOM (Danilov et al., 2015). The employed thermodynamic approach utilizes a zero-layer thermodynamic module (Parkinson & Washington, 1979), with constant dry and melting albedos of ice and snow. In the simulation of the Great Lakes ice formation process, both SCHISM and single-class ice model allow multi-scale physics on variable resolution, but the rate of melting within the model is more rapid than what has been observed (Zhang et al., 2023). In order to improve the simulation capability of ice, the implementation of the multi-class sea ice module, Icepack, is required.

When Icepack is coupled with another model, the latter must implement its own transport solver for ice. Hunke et al. (2010) suggested that the solver should be accurate, stable, conservative, strictly monotonic, and efficient. In the sea ice model, monotonicity ensures that the values of new tracers do not exceed the local extrema, specifically the maximum or minimum values in their vicinity under pure advection (Lipscomb and Hunke, 2004). For ice concentration, it can exceed 1 and results in ridge which has been described in Icepack. With the advancement in High Performance Computing, sea ice coupled models are

increasingly ~~executed on higher spatial and temporal resolutions. The increased demand for resolution and complexity in the sea ice models calls for an accurate, stable, conservative, strictly monotonic, and efficient sea ice transport method (Hunke et al._2010).~~ The methodology for sea ice transport has undergone extensive study over the years, resulting in the proposition of various schemes.~~The sea ice transport method has been studied for many years, and various schemes have been proposed.~~ Lipscomb and Hunke ~~et al.~~ (2004) implemented the upwind and incremental remapping schemes in CICE, both of which are still available in the latest version. Although the upwind scheme stands as the simplest method for transport, its first-order accuracy results in excessive diffusion.~~The upwind scheme is the simplest scheme for transport, but it is too diffusive due to its first order accuracy.~~ The incremental remapping scheme is a second-order accurate scheme, and has great performance in structured grid models, but requires excessively smaller time step to avoid cross trajectories for highly distorted UGs.~~but is inefficient for highly distorted UGs.~~ For example, MPAS-Seaice uses the incremental remapping scheme (Turner et al., 2022) ; however, as it is a global model, it typically operates with coarser resolution,~~ but as a global model, its resolution is usually coarse.~~ The MITgcm provides a variety of tracer advection solvers, with a recommendation for flux-limited schemes in order to prevent unphysical outcomes ~~MITgcm offers many tracer advection solvers, but it recommends flux-limited schemes to avoid unphysical results~~ (Adcroft ~~Campin~~ et al. 2023). NEMO uses either the Prather scheme or the ULTIMATE-MACHO scheme with SI^3 ice model (~~Gurvan~~ Madec et al., 2022), both of which require some functions to limit the tracer concentrations from exceeding the largest values of all adjacent nodes. ~~The efficiency has not been well tested on those SG models under very high resolution down to about tens of meters.~~

In the case of triangular UGs, the transport scheme utilized in UG-CICE is the second-order upstream scheme, which considers the gradient of sea ice tracers (Gao et al., 2011). This scheme is consistent with the tracer transport in FVCOM (Chen et al., 2012). ~~It is unclear if the monotonicity is guaranteed by this scheme or if additional diffusion is needed.~~ The transport scheme of FESOM2 is the ~~Finite Element Flux Corrected Transport scheme (~~FEM-FCT ~~;~~ (Löhner et al., 1987), which is based on the finite element description (Danilov et al. 2015). It is also a conservative and second-order scheme (Budgell, et al. 2007), but its cost is linearly increasing with the number of variables, and more importantly, strict monotonicity comes with a higher cost (Löhner et al., 1987). It is imperative to underscore that the requirement for strict monotonicity is designed to prevent unphysical values that can crash the model. Therefore, Zhang

et al. (2023) used the ~~upwind~~ modified FEM-FCT scheme by zeroing out certain ~~the~~ higher-order contribution in their study for single-class ice module with very high resolution.

~~SCHISM, which has the seamless cross-scale capability from creek to ocean (Zhang et al., 2016), has been applied to study the Great Lake ice formation process and obtained reasonable results in very high resolution (Zhang et al., 2023), using a single-class ice/snow module borrowed from FESOM (Danilov et al., 2015). The thermodynamics employed is a 0-layer thermodynamic module (Parkinson & Washington, 1979), with constant dry and melting albedos of ice and snow. In the simulation of The Great Lake ice formation process, both SCHISM and single-class ice model allow multi-scale physics on variable resolution (Zhang et al., 2023). However, the performance of the multi-class sea-ice formulation has not been tested before. SCHISM therefore represents a mature and reliable platform to implement the multi-class sea ice module, Icepack.~~

This paper presents SCHISM-Icepack, a~~n new~~ unstructured ice-ocean coupled model that updates ~~built on~~ SCHISM ~~and~~ for Icepack~~.~~. The coupled model utilizes the TVD transport ~~scheme~~ scheme, which has been implemented in SCHISM for ocean tracers (Zhang et al., 2016), to achieve an efficient, strictly monotone, second-order accuracy scheme for ice tracers on generic unstructured grids (even with locally very high resolution). Section 2 introduces components of SCHISM-Icepack~~the coupled model~~ and describes how the TVD transport scheme is implemented for the ice model. In Section 3, we compare some ideal test results from the new TVD scheme with two other second-order accurate methods (the second-order upwind scheme and FEM-FCT~~the upwind scheme and a central difference scheme~~). The efficiency of the TVD scheme is also compared with the upwind scheme when applied to a high-resolution mesh. Additionally, the results of the new coupled model are compared with those of the existing single-class ice model of SCHISM. The new coupled model is validated with a simulation of the Arctic Ocean sea ice using realistic atmosphere ~~and compare the efficiency with upwind scheme when applied to a high-resolution mesh; we also validate the new coupled model with a simulation of the Arctic Ocean sea ice with realistic atmosphere forcing. Section 4 compares the new TVD scheme with other TVD schemes. Section~~ forcing. Section ~~5~~ 4 summarizes the major findings of this work.

2 Method

2.1 Icepack implemented in SCHISM

~~SCHISM-Icepack is~~We coupled by Icepack v1.3.4 (Hunke et al., 2023) ~~with~~ and SCHISM v5.11. Besides the ~~0~~zero-layer thermodynamics, two more sophisticated thermodynamic formulations, BL99 and the mushy layer are also implemented. At the sub-grid scale, thin and thick ice coexist, and therefore an ice thickness distribution (ITD, Lipscomb, 2001~~,~~; Bitz et al., 2001; Bitz and Lipscomb, 1999) has been implemented in order to describe the unresolved spatial heterogeneity of the thickness field. The ITD offers a prognostic statistical description of the sea ice thickness, which it divides into multiple categories, along with the ice area fraction corresponding to each category – a more detailed approach than the singular fraction used in the previous implementation. ~~The ITD provides a prognostic statistical description of the sea ice thickness partitioned into multiple categories and of the ice area fraction associated to each category, instead of only one fraction as in the previous implementation.~~ More tracers and more ice processes are added in this ~~new version of~~ coupled model by Icepack, including multiple melt pond~~s~~ parameterizations (Hunke et al., 2013) and a mechanical redistribution parameterization (Lipscomb et al. ~~Hunke~~ 20~~07~~10) that responds to sea ice convergence by piling up thin sea ice and therefore mimicking ridging and rafting events. The interaction between the shortwave radiation and the sea ice in Icepack is addressed using two formulations:~~is described by~~ the ~~'~~Community Climate System Model (CCSM3)~~'~~ formulation, which relates ~~links~~ the surface albedo to the surface sea ice temperature, and ~~or~~ the Delta-Eddington formulation (Briegleb et al., 2007), which relates ~~links~~ the albedo to inherent optical properties of sea ice and snow. The dynamic solver is not included in Icepack and is based on two approaches: 1. ~~a~~ the classic Elastic-Viscous-Plastic method (EVP, Hunke & Dukowicz, 1997), and 2. the modified Elastic-Viscous-Plastic method (mEVP, Kimmritz et al., 2015~~),~~). ~~B~~both methods are inherited from the ~~old~~ previous single-class ice/snow formulation (Zhang et al. 2023). It is important to note the difference in grid definition between the ice module and the hydrodynamic module. The ice module uses the Arakawa-A grid, and all tracers and velocities are defined at nodes, while the hydrodynamic module uses the Arakawa-CD grid. The decision to employ an analogue of the Arakawa-A grid in the rheology part, adapted from FESIM, was primarily based on its computational efficiency and success in sea ice simulation (Danilov et al., 2015). All ice-related subroutines are called at each time step in the ocean model~~every ocean step~~ by SCHISM's hydrodynamic core. The ice module exports to SCHISM variables

needed for coupling such as the shortwave radiation, the ice-ocean heat flux, the freshwater flux, and finally the sea ice pressure and ice-ocean stress for all ice-covered nodes, in proportion to the sea ice area fraction. Over open ocean these variables are calculated directly by SCHISM. All variables required by Icepack can be obtained from either SCHISM or separate input file. And es.the coupling between the ice module and the hydrodynamic module remains unaffected by the differences in the variable definition, as all forcing variables are located at nodes in the hydrodynamic module.

2.2 Schemes for sea ice transport

The basic transport equation of sea ice area or fraction a_n for each sea ice category is (Thorndike et al. 1975),

$$\frac{\partial a_n}{\partial t} + \frac{\partial u a_n}{\partial x} + \frac{\partial v a_n}{\partial y} + \frac{\partial}{\partial h}(a_n f) = \psi, \tag{1}$$

wWhere u and v are the ice velocities of x and y components, respectively, and h is the ice thickness. The last term on the left side is thermodynamic change, where f is the rate of ice melting or growing, and the right-side term ψ is mechanical redistribution like the ridging process. We solve this equation using a fractional step method: first solve a pure advection equation (i.e. by setting the thermodynamic term and mechanical redistribution term to 0), followed by a correction step that includes the remaining terms. The main challenge occurs in the first step, where we must solve a pure advection equation for one category of sea ice fraction a_n:

$$\frac{\partial a_n}{\partial t} + \frac{\partial u a_n}{\partial x} + \frac{\partial v a_n}{\partial y} = 0. \tag{2}$$

NNote —that the ice velocity field is divergent or convergent, which can produce new local maxima/minima. However, a strictly monotone scheme is still desirable in order to separate the numerical dispersion from the physical convergence.

We apply a finite volume algorithm to discretize equation (2). Unlike the Arakawa CD grid used in SCHISM, theThe sea ice module inside SCHISM employs an Arakawa-A grid, with both the sea ice velocity and tracers located at the node (blue circles in Fig.1). The tracer control volume is defined as the polygon enclosed by the lines composed of centroids and edge centers (red circles in Fig.1). So, in

the subsequent time step, after Δt, the new ice fraction is:

$$a_n^{t+1} = a_n^t + \frac{\Delta t \sum_{i \in S} Q_i \phi_i}{\Omega_S}, \tag{3}$$

Ω_S is the total area of the control volume; S is its boundary, and Q_i is the flux across the edge i of the control volume. Most of these variables can be obtained easily in the model, so we only focus on finding a method to proximate the edge tracer value, ϕ_i.

The simplest method is the first order upwind scheme (assuming, without loss of generality, the velocity direction is as depicted in Fig. 1):

$$\phi_i = \phi_{C.5} \tag{4}$$

~~The central difference scheme is~~

~~$$\phi_i = \frac{1}{2}(\phi_C + \phi_D), \tag{5}$$~~

~~Where ϕ_C and ϕ_D are the values at the upwind and the downwind nodes, respectively, for one edge of the control volume (Fig.1a).~~

The TVD corrects the upwind values as:

$$\phi_i = \phi_C + \frac{\psi_i}{2}(\phi_D - \phi_C), \tag{$\cancel{6}5$}$$

where ϕ_C and ϕ_D are the values at the upwind and the downwind nodes, respectively, for one edge of the control volume (Fig.1a). And t~~T~~he last term on right side is the anti-diffusion correction. In this part, ψ_i is a function of the upwind ratio, r_i, for which we select the v~~V~~an-L~~l~~eer limiter (van Leer, 1979),

$$\psi_i = \frac{r_{i*} + |r_i|}{1 + |r_i|}, \tag{$\cancel{7}6$}$$

$$r_i = \frac{\phi_C - \phi_{U*}}{\phi_D - \phi_C}_{.5} \tag{$\cancel{8}7$}$$

If $r_i < 0$, it means ϕ_C is a local extreme, ϕ_i in Eq.6 will revert to upwind.~~;~~ I~~i~~f $r_i > 0$, there is no local extreme, so ϕ_i is a weighted average of ϕ_C and ϕ_D. And here,~~Where~~ , ϕ_{U*} is defined as the upwind node of the upwind node (i.e., 'up-upwind'), and can be accessed easily in a structured grid or a uniform unstructured grid (Fig.1a). But for generic unstructured grids, how to approximate ϕ_{U*} is a key issue for the TVD scheme. There are several possible choices for ϕ_{U*}, and after some comparisons we choose the method proposed by Darwish et al. (2003). This method includes the gradient of the central node $\nabla \phi_C$.

$$\phi_{U*} = \phi_D + R_{DU} \cdot (\nabla \phi_C) = \phi_D - 2R_{CD} \cdot (\nabla \phi_C), \tag{$\cancel{9}8$}$$

where R_{DU} is the vector from the downwind node to the up-upwind node, and R_{CD} is the vector from the upwind to downwind nodes.
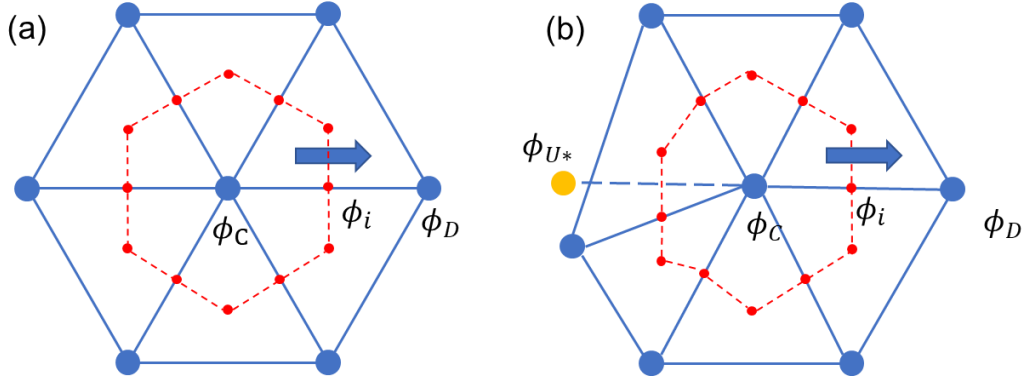
Figure 1. Schematics of control volume for the ice transport; **(a)** is for a uniform unstructured mesh, **(b)** is for a generic unstructured mesh.

As the sea ice concentration cannot exceed 1 or be negative in this pure advection step (but after the transport step, it can exceed 1 and lead to the ridging process, and in the latter case, Icepack will perform clipping), Darwish's method (9) can produce errors and needs to be limited:

$$\phi_{U*} = \min\left(1, max\left(0, \phi_D - 2R_{CD} \cdot (\nabla\phi_C)\right)\right),$$

(~~10~~9)

Using the approximation of edge tracer values ϕ_i~~ϕ_{U*}~~, we can calculate the sea ice area fluxes across every edge of the control volume, and thus the new concentration from Eq. (3). Other tracer fluxes like volume per unit area of ice and enthalpy depend on the area fluxes, as ~~does~~ in CICE. For instance, the volume per unit area of ice v_n equals the product of the sea ice area a_n and the sea ice thickness h_n, here h_i is the sea ice thickness of the upwind node.

$$v_n = a_n h_n,$$

(~~11~~10)

$$v_n^{t+1} = v_n^t + \frac{\Delta t \sum_{i \in S} Q_i \phi_i h_i}{\Omega_S},$$

(~~12~~11)

Sea ice enthalpy e_n is the product of the sea ice area a_n, the sea ice thickness h_n and the energy per unit volume q_n, here q_i is the energy per unit volume of upwind node.

$$e_n = a_n h_n q_n,$$

(~~13~~12)

$$e_n^{t+1} = e_n^t + \frac{\Delta t \sum_{i \in S} Q_i \phi_i h_i q_i}{\Omega_S},$$

(~~14~~13)

OOther tracers at the new step can be calculated this way.

The finite-volume method ensures both global and local conservation of tracers. Since all ice area fluxes are recorded, the method requires only a single flux calculation per ice category, enhancing computational efficiency.Given that all ice area fluxes are recorded, flux calculation within the same category of ice only needs to be done once, so the method is computationally efficient. Numerous tests have demonstrated that the TVD scheme provides second-order accuracy in smooth regions (Zhang et al., 2015), and guarantees strict monotonicity and a good accuracy. The limiter for this studywe chose is the widely used Vanvan-Lleer limiter. Even though the accuracy of this limiter may be locally reduced to first order, it always maintains monotonicity as long as the time step used satisfies the stability condition, as demonstrated by Sweby (1984). Sea ice concentration can exhibit new extremes after the transport step as a result of physical processes such as convergence and divergence.Sea ice concentration may produce new extremes after the transport step due to convergence Furthermore, the monotonicity of tracers . However, it should never be negative; this is guaranteed because the method in Eq. (311) and Eq. (13) is essentially a weighted average method with non-negative weights.

3 Results

3.1 Idealized test case

Since the thermodynamic part and dynamic parts of this model are relatively mature and have been widely utilized in other models, in this study we focus on validating the new transport scheme. The comparison of a fewseveral transport schemes is carried out through an idealized ice transport experiment in a uniform unstructured mesh. The mesh grid consists entirely of equilateral triangles, with a side length of 200m for each triangle. As the initial condition, we placed a rectangular sheet of sea ice with dimensions of 5000m x 5000m on the left side of the mesh. The initial ice thickness is 1.5m, and it moves to the right along the x-axis at a speed of 1m/s. The time step is 1 second, which satisfies the Courant-Friedrichs-Lewy condition of TVD (Zhang et al., 2016). We run the idealized experiment for 24 hours, equivalent toor 86400 steps. We select two other second order transport schemes for comparison,-: the first second-order upwind scheme referred to UG-CICE -(Gao et al., 2011) and the the central difference scheme (with proper limiting based on local max/min)FEM-FCT scheme. It should be noted that in UG-CICE, although tracers are positioned at vertices (nodes) as in our model, the velocity

is calculated at the centroids, differing from our scheme. The skill metrics employed include the accuracy and the monotonicity of the results.The skill metrics include the accuracy, conservation, and monotonicity of the results.

3.1.1 Accuracy

Fig. 2 shows the snapshots and corresponding central profiles along the x-axis of the sea ice concentration taken every 3 hours, with the theoretical solution represented by the red rectangles. For clarity, only areas with a concentration greater than 15% are shown. Compared to other schemes, the second-order upwind scheme exhibits significantly higher diffusivityis significantly more diffusive, yet relatively uniform. The shape of the ice distribution varies over timeThe outline varies in shape, transitioning from a square to a circle. By the conclusion of the model run, the peak ice concentration reduces to roughly 20% of its initial value—this is the lowest retention observed amongst the three schemes. Moreover, most nodes fall below the 15% concentration visibility threshold in the snapshot.At the end of the model run, the peak of ice concentration is approximately 30% of the initial value, which is unsurprisingly the lowest among the three schemes. The central difference schemeFEM-FCT scheme retains more most sea ice in the red rectangle than the upwind scheme. However, while it produces non-uniform results even though the ice speed is uniform, and it requires clipping of under/overshoots (which violates the conservation). Some sea ice is left behind, with a banded distribution along the x-axisat the trailing and leading edges (Fig. 2b). The profiles portrayed in Fig. 2e indicate that the peak of sea ice concentration exhibits multiple peaks while the peak ice concentration consistently approaches 100%reaches approximately 90% in the end and is the sharpest result of the three schemes. Figs. 2c and 2f demonstrate that the TVD scheme matches the FEM-FCT's accuracyhas the best accuracy compared to the other two schemes, and better than that of the second-order upwind scheme. Moreover, tThe horizontal distribution of the ice is closest also close to the analytical solution and exhibits a peak ice concentration around 100% at all times, despite some minor diffusion at the frontal edges, akin to the FEM-FCT scheme.on the frontal edges.
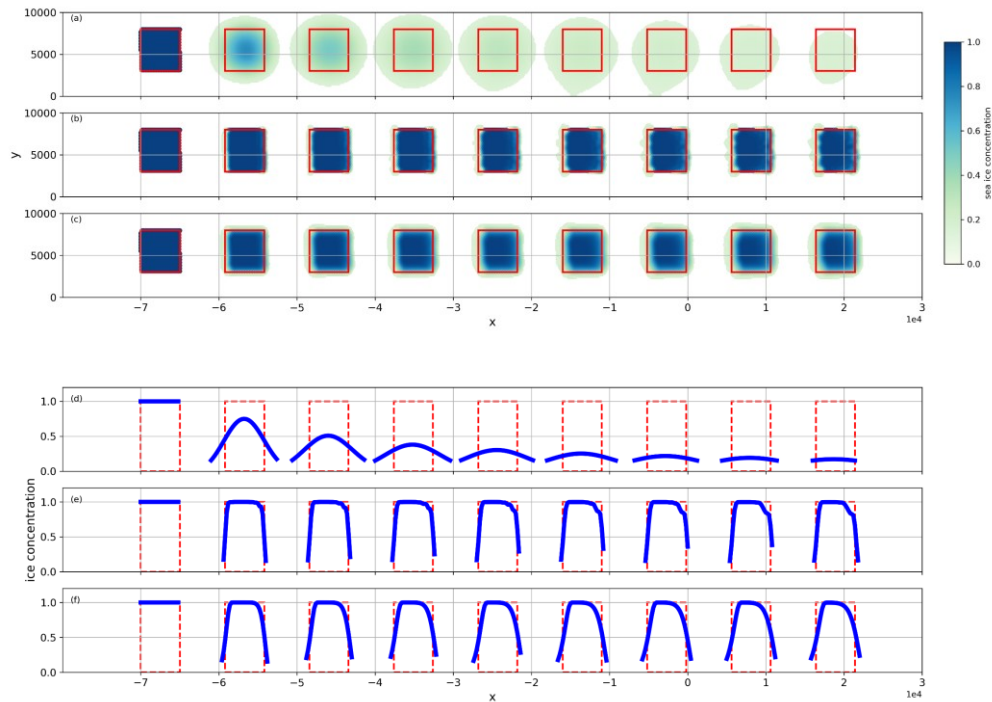
305

Figure 2. Sea ice concentration snapshots **(a-c)** and profiles **(d-f)**. The sea ice moves from left to right, snapshots are taken every 3 hours, and the red rectangular is the exact solution. **(a, d)** second-order upwind, **(b, e)** FEM-FCT, **(c, f)** TVD ~~(a, d) Upwind, (b, e) Central difference, (c, f) TVD.~~

310   The results of the ice volume per unit are analogous to the patterns observed in ice concentration~~area are similar to the ice concentration~~ (Fig. 3). Among the tested schemes, ~~T~~the second-order upwind scheme is the most diffusive one~~. The~~, while the peak of ice volume per unit area is only 0.~~4~~3 meters at the end. ~~The central difference scheme is superior to the upwind scheme, and there is no excessive~~

315   ~~amount of ice that lies outside the red rectangle on the top, bottom, and front edges. However, the scheme still shows multiple peaks in Fig. 3e. Furthermore, it has obvious overshooting in all snapshots, which can be attributed to some spurious convergence processes that should not have occurred. T~~The FEM-FCT and TVD schemes both demonstrate comparable accuracy~~he TVD scheme is the best of the three schemes. It performs well,~~ ~~maintaining in terms of both~~the shape and its peak value. From commencement to conclusion, the geometries of the ice volume per unit area closely resemble the

320   theoretical model, with the peak values for TVD (1.496m) and FEM-FCT (1.495m) finishing marginally below the precise solution.~~The shape of the ice volume per unit area is close to the theoretical solution from start to finish, with the peak value slightly (1.496m) lower than the exact result at the end.~~ The ice volume per unit profiles of the three schemes (Fig. 3d-f) exhibit shapes

analogous to those seen in the ice concentration (Fig. 2d-f), suggesting all schemes largely preserve monotonicity. However, the FEM-FCT scheme exhibits non-monotonic behavior at the ice edges, and this will be further discussed below. ~~The ice volume from the upwind and TVD (Fig. 3d and f) has similar shapes to the ice concentration (Fig. 2d and f), indicating that both schemes maintain the monotonicity well,~~ itand ~~we will discuss more on this later.~~
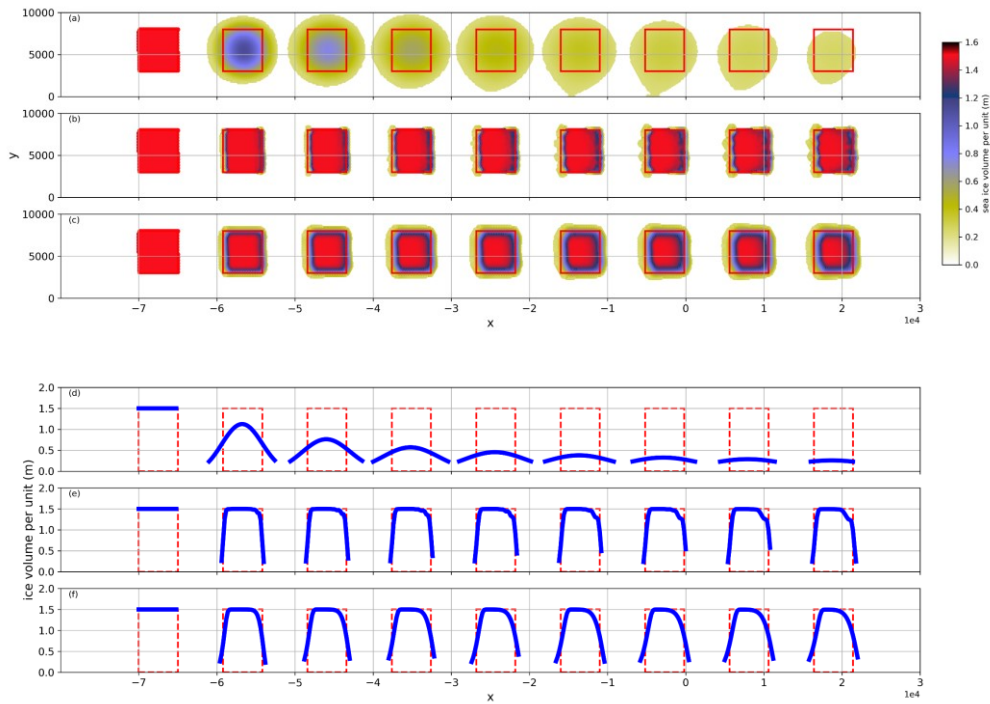
Figure 3. Volume per unit area of ice, with snapshots **(a-c)** and profiles **(d-f).** The sea ice moves from left to right, snapshots are taken every 3 hours, and the red rectangular is the exact solution. **(a, d)** ~~Upwind~~second-order upwind, **(b, e)** ~~Central difference~~FEM-FCT, **(c, f)** TVD

~~**3.1.2 Conservation**~~

~~We assess the conservation property of schemes using two parameters to determine whether there is a loss or increase in sea ice area during transport. The first parameter is the ratio of the total ice area after transport to the initial total ice area. The second parameter is the ratio of the ice area that reaches the target area to the theoretical solution, which also indicates the degree of accuracy. In Table 2 we can see that, for the total area of ice, there is no change in area during the transport process using the upwind and TVD schemes. In contrast, the ice area of the central difference scheme declines initially, and then increases over time. This suggests that the limiting procedure used in the central difference scheme destroys conservation. The upwind scheme performs relatively well at first, with ~72.34% ice reaching~~

~~the target area after 1 hour. But its performance drops significantly, to ~25.76% at the end. The central difference scheme, achieves a percentage of ~60.29% at first, and at the end it manages to achieve ~55.11%. Among the three schemes, TVD is the most effective with a consistently higher percentage compared to the others. The percentage of the region reaching the target area exceeds 90% after 1 hour and consistently maintains a rate of nearly 80% towards the end.~~

		~~1 hour~~	~~3 hours~~	~~6 hours~~	~~12 hours~~	~~24 hours~~
~~Upwind~~	~~All area~~	~~100.00%~~	~~100%~~	~~100%~~	~~100%~~	~~100%~~
	~~In the target area~~	~~79.41%~~	~~65.71%~~	~~53.62%~~	~~39.40%~~	~~25.76%~~
~~Central difference~~	~~All area~~	~~72.34%~~	~~77.85%~~	~~80.92%~~	~~85.50%~~	~~91.82%~~
	~~In the target area~~	~~60.29%~~	~~59.08%~~	~~58.88%~~	~~57.08%~~	~~55.11%~~
~~TVD~~	~~All area~~	~~100.00%~~	~~100%~~	~~100%~~	~~100%~~	~~100%~~
	~~In the target area~~	~~91.23%~~	~~88.12%~~	~~85.67%~~	~~83.14%~~	~~79.22%~~

~~**Table2.** Ice area as a percentage of the exact solution.~~

3.1.2~~3~~ Monotonicity

Here we select the ice thickness as the representative of trace~~r~~s to verify monotonicity, with the ideal transport scheme expected to maintain the initial ice thickness (1.5m). Fig.~~2c~~ 2d and Fig.~~3c~~ 3d have shown the ~~central~~ second-order upwind is~~difference is not monotone~~ overly diffusive, ~~as the ice thickness per unit area exceeds the initial maximum even in the first snapshot (3 hours after the start of the case);~~ so we exclude it in the current comparison. Considering that non-monotonicity typically occurs in areas of low ice concentration,~~Given that the non-monotonicity usually happens at low concentration areas,~~ we choose 0.1% as the threshold. In most areas,~~The~~ the ~~upwind~~ FEM-FCT scheme maintains monotonicity, ~~is completely monotone~~ and the ice thickness remains consistent with the initial value (Fig. 4a). But at the leading edge of the ice, the thickness overshoots the initial value and oscillates at the trailing edge. For the TVD scheme, some overshoots would occur at the leading edge~~in the forward edge~~ of ice (Fig.4b) if we did not limit the up-upwind value (cf. Eq. 9~~8~~). On the other hand, the ~~new~~ modified TVD scheme we developed that limits the up-upwind value (cf. Eq. (10~~9~~)) is completely monoton~~e~~ic (Fig. 4c).
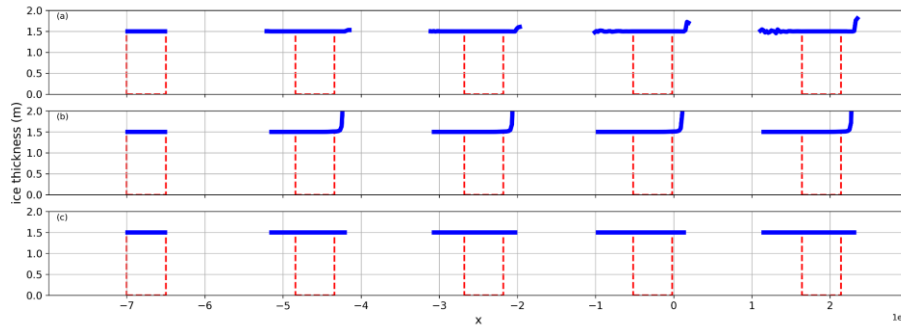
Figure 4. Sea ice thickness calculated from **(a)** ~~Upwind~~FEM-FCT, **(b)** original TVD (Eq. (9~~8~~)), **(c)** ~~new~~ modified TVD (Eq. (1~~0~~9)) for ice. The time interval of snapshots is every 6 hours.

In summary, we have demonstrated that the TVD scheme provides second-order accuracy and outperforms that of the second-order upwind method. Although the FEM-FCT method could be more accurate than the TVD scheme, its propensity for non-monotonicity can cause numerical overshoots, consequently leading to unphysical values for salinity or temperature of ice, which might result in model instabilities or even 'blowup'. Approaches to enforcing the monotonicity in the FEM-FCT method may entail higher cost (Löhner et al., 1987) or lower accuracy (Zhang et al.,2023). On the other hand, the TVD scheme not only preserves the tracer monotonicity but also meets other requirements such as accuracy, and we will further test its efficiency in a realistic case.

3.2 Realistic model run

SCHISM-Icepack, in conjunction with the TVD scheme for its ice transport module,~~A realistic ocean-ice coupled model using the TVD scheme for the ice module~~ is ~~developed~~ employed to reproduce the ice processes in the Lake Superior and the Arctic ~~Ocean~~Ocean (Fig.5). The ~~In contrast to the idealized case, both meshes are non-uniform (Fig.5), so the~~ successful tests on unstructured ~~demonstrate~~grids demonstrate the cross-scale capability of SCHISM-Icepack~~the coupled model~~.

3.2.1 ~~Test on~~The Lake Superior case~~a very high-resolution mesh~~

To gauge the numerical efficiency of the new TVD scheme, we test it on a very fine resolution Lake Superior mesh (Fig.5a) that was previously used in Zhang et al. (2023). The nearshore resolution in this mesh reaches ~50m with the finest resolution of 41.5m, found on the southwestern shore. As Zhang et al. (2023) indicated, the FCT scheme was having stability issues, so an essentially upwind method was

applied in the high-resolution areas. The performance is compared with the upwind scheme. We

390 simulate the case for 180 days from December 1st, 2017, using 48 60 processors. The total simulation

times for the two schemes are comparable are similar with 2 schemes, 637 678 minutes for the TVD

scheme and 654 675 minutes for the upwind scheme. In total, the upwind scheme consumes 52.39 core

hours while TVD spends 54.56 core hours. Compared to the total time of the ice module, TVD

accounts for 21.71% and upwind accounts for 21.01%, while the dynamic part is the most

395 computationally intensive, accounting for more than 70%. Note that the upwind scheme would be

cheaper, but the total times shown include other modules in the model; the diffusion in the upwind

scheme has led to a larger ice coverage area, thus increasing the cost of the ice solver. Overall, we

found that the computational cost of the cost for the TVD scheme is comparable to that of the upwind

scheme for many in this realistic benchmark applications.
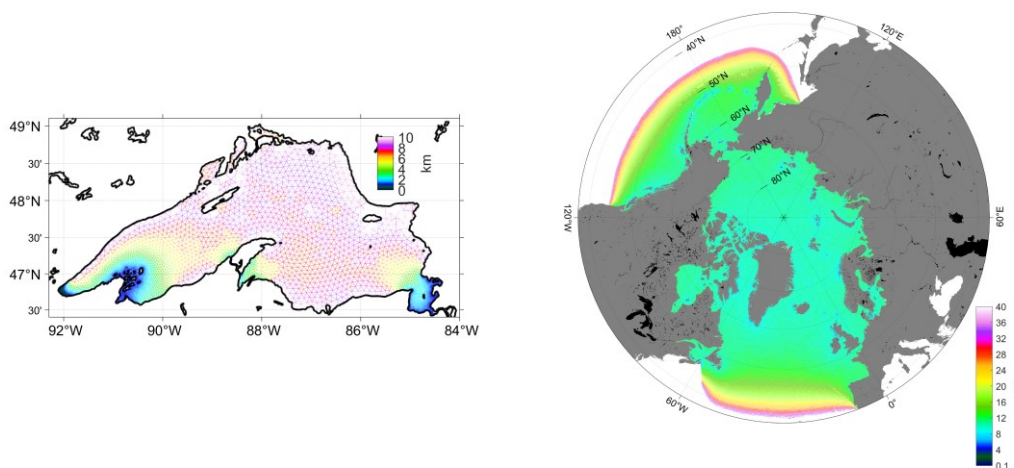
400

Figure 5. (a, left) The Lake Superior mesh. **(b, right)** The Arctic Ocean mesh. The colors show the mesh resolution.

As we have mentioned before, Then we compare the result with the previous version, the single class

ice model in this case (Fig. 6). Zhang et al. (2023) have used a single-class ice model to reproduced the

405 seasonal and interannual variability of ice extent well (the ice concentration greater than 15%) in this

case. The simulation results has have been , which compared to the Great Lakes Surface Environmental

Analysis (GLSEA) data, including some rapid melting-refreezing events. But they also found in their

model that ice melts excessively fast near the end of each melting season of each year. Here we

compare the ice extent and ice concentration between two models. With the multi-class ice model and

410 the TVD scheme, For ice extent, i we are able to reproduce the similar pattern of ice extent and also

some rapid melting-refreezing events, yielding a correlation coefficient of 0.93 and a Wilmot score of

0.92 (Fig. 6).~~with being~~being Furthermore, the melting phase simulation is improved beyond day 120.~~.,~~ Approximately 10,000 km² of ice persists until around day 150 and the ice dissipates by day 160, aligning more closely with observational data.~~T~~ After the observed ice extent falls below 10,000 km², the correlation coefficient using the multi-class ice model is 0.82, which is an improvement over the single-class ice model's coefficient of 0.43.~~0.43 forsingle-class ice model~~
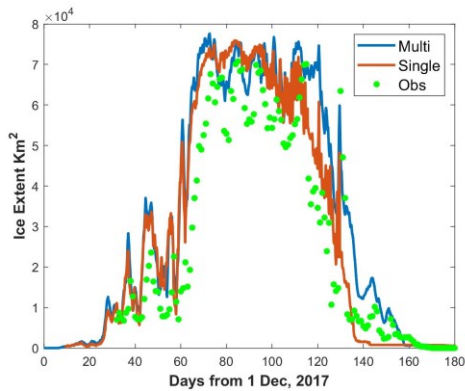
Figure 6. Comparison of ice extent in Lake Superior in 2017, the blue line is the result of multi-class ice model, the orange line is the result of single-class ice model, and green dot is the observation from GLSEA.

The spatial distribution of the ice concentration from the two models is compared with the observation from the U.S. National Ice Center (USNIC) on day 90 (Fig.7), when the ice cover was largest. ~~Next, we qualitatively compare results ice concentration from betweenthe two schemess on Day 100 (Fig.6), when the ice cover is largest. The Rresults of for ice concentration are similarshow both similarities and differences between the two models, t~~Both models exhibit lower ice concentration in the southern part of the lake; however, while in most other areas, particularly in the western region, the multi-class ice model displays lower ice concentrations.~~Twith higher concentration in the nearshore area and lower concentration in the center of the lake, which is consistent with the single-class ice model of Zhang et al. (2023). The TVD results reveal more variability especially in the open water. The results for the ice thickness are quite different, with thick ice further from the coast from the upwind result than from the TVD scheme (Fig. 6).~~Compared to the USNIC data, both models overestimate ice concentration on the lake's eastern side. However, the multi-class ice model~~new version~~ reproduces the ice-free pattern on the west coast more accurately. The spatially average ice concentration is 0.617 for the multi-class ice model, which is closer to the observed value of 0.509 and represents a significant improvement over the single-class ice model's 0.847~~is much betterresult of the single-class ice model. This is because the upwind scheme is more diffusive than TVD.~~ In the very high-resolution areas (the lake's southwestern

and southeastern corners) ~~(southwestern and southeastern corners)~~, the new coupled model and ~~the~~ TVD~~both~~ scheme~~s~~ yield a reasonable and stable result~~s~~, which demonstrates ~~the coupled model's~~ its cross-scale capability~~, as in the single-class version~~.
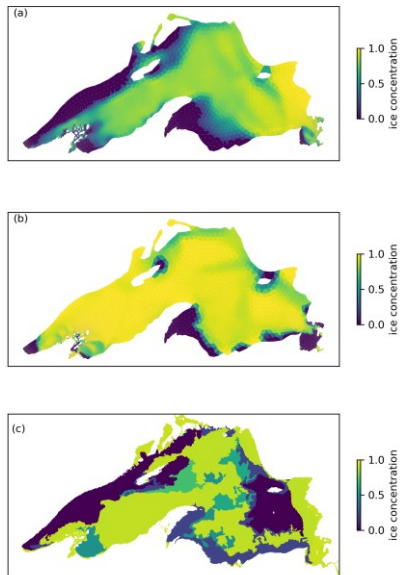
440

Figure 6_7_. T~~he top row is t~~he ice concentration ~~at~~ on ~~Day~~ day ~~100~~90, and **(a)** is the result of the ~~upwind~~ multi-lass ice model~~scheme~~ **(e_b_)** is that of ~~the TVD scheme~~single-class ice model. ~~The bottom row is the ice thickness per unit and~~. **(b_c_)** is ~~for upwind, (d) is for TVD~~from USNIC.

445

3.2.2 ~~Test on t~~The Arctic Ocean case

The Arctic mesh consists of 422,000 elements and 217,000 nodes (Fig. 5b) with the resolution ranging from 6 km near the coast to 40 km at the open boundary. The model starts on January 1st, 1994, and covers 2000 days, about 1.6 million steps using a time step of 100 sec.~~N.~~ Initial conditions are derived from the~~The initial condition is obtained from~~ HYCOM dataset, including ocean tracers, sea ice concentration and thickness. Moreover, the boundary conditions incorporate data~~the boundary condition is obtained~~ from HYCOM and Finite Element Solution (FES2014, Lyard et al., 2021), including 15 tidal components. The domain boundary is chosen to be at ~40°N to ensure no sea ice crosses the boundary. In the vertical dimension, a highly flexible vertical gridding system (LSC^2, Zhang et al., 2015) ~~has been~~is implemented with up to 60 layers in order to more accurately represent

~~describe~~ the complex topography of the Arctic Basin better, and we set the bottom drag coefficient with a constant ~~manning~~ Manning coefficient ~~at~~ of 0.0~~0~~25. For the atmosphere forcing, we choose ~~The~~ the European Centre for Medium-Range Weather Forecasts Reanalysis Fifth Generation global reanalysis (ERA5, Hersbach et al., 2020) ~~due to~~ for its high temporal resolution, and ~~use~~ utilize the bulk aerodynamic model (Zeng et al., 1998) to get the surface fluxes, like latent and sensible fluxes. The turbulence closure scheme in the ocean ~~hydro~~ model is the generic length-scale equation as k-kl (Umlauf and Burchard, 2003) and the horizontal transport in the ~~hydro m~~ocean model is TVD^2 (Ye et al. 2016). The parameters used in the sea ice model basically follow the standard CICE configuration, including a constant air-ice drag coefficient (about 0.0016), and a constant ice-ocean drag coefficient (about 0.006). Modules in the standard CICE are also included in this model, ~~e.g.,~~ such as the mushy layer thermodynamics, the Rothrock (1975) ice strength method, and the level-ice melt ponds module~~, etc~~ among others. We evaluate our Arctic sea ice case by comparing its outputs to observational data sets from ~~We compare the results of our Arctic sea ice model with the~~ NSIDC ~~observation~~, including the sea ice extent, ice boundary, and ice concentration. The observation of ~~Sea~~ sea ~~Ice~~ ice ~~Concentrations~~ concentrations is from Nimbus-7 SMMR and DMSP SSM/I-SSMIS Passive Microwave Data (Fetterer et al., 2017), while the sea ice boundary corresponds to the 15% sea-ice concentration contour.

Fig.~~7a~~ 8a compares the sea ice extent of SCHISM-Icepack ~~our model~~ with the observation. The model is stable for the long-term test and has good performance to reproduce the inter-annual variability and the seasonal cycle, with both the minimum and maximum sea ice extents~~the minimum and maximum~~ being reproduced satisfactorily. The first peak is noticeably higher than the observed value, which may be influenced by the initial conditions as we did not get all tracers, such as sea ice salinity and enthalpy, from HYCOM. The extent difference between the model and observation is evaluated as absolute extent error (AEE, Eq. ~~15~~14). However, AEE may underestimate the model error due to the cancellation between the overestimation(O) and underestimation(U). The Integrated Ice Edge Error (IIEE, Eq. ~~16~~15) may be a preferable choice to evaluate the simulation result (Goessling et al., 2016, Zampieri et al., 2018).

$$AEE = |\textstyle\sum(|O| - |U|)|, \tag{$\cancel{15}$14}$$

$$IIEE = \textstyle\sum|O| + \sum|U|, \tag{$\cancel{16}$15}$$

485 We present the monthly AEE and IIEE in Fig. ~~7b~~8b, provide monthly statistics for them and compare

our results with those from the FESOM2~~'s~~ in Fig. ~~7c~~8c. FESOM2 team has run multiple cases to

investigate the sensitivity ~~e~~ of results to various forcing and model complexities, and selecting cases for

our comparison that ~~the ones we selected~~ were also driven by ERA5 and based on a multi-class ice

thermodynamics BL99 (Zampieri et al., 2021). IIEE and AEE (Fig. ~~7b~~8b) fluctuate in a similar fashion

490 to the monthly extent in Fig.~~7a~~8a. In Fig.~~7a~~8a, the simulated sea ice extent often increases more rapidly

~~faster~~ during autumn compared to observed data~~in autumn than observation~~, and it appears to more

closely match observations ~~seems to perform better~~ in ~~other~~ the remaining seasons. AEE shows a similar

pattern, being relatively small in spring and summer, and reaching its maximum in autumn. The

magnitude of AEE is also similar to that of FESOM2, peaking in autumn while lower in other seasons.

495 The seasonal pattern of IIEE is similar to that of FESOM2, with maximum values during summer and

lower values during autumn. Correspondingly, T~~t~~he largest variability of IIEE occurs in summer,~~ too,~~

while the lowest variability is observed in spring. The differences between SCHISM-Icepack ~~our model~~

and FESOM2 can be attributed to two primary factors: ~~may be caused by two factors. T~~the first is that

the selected FESOM2 results ~~we select to compare from FESOM2 use~~employed a different

500 thermodynamic module and the second is that the integration period of FESOM2 ~~is~~ spanned from 2002

to 2015, while ~~this study's~~ integration period of this study ~~–~~is from 1994 to 1999. Nonetheless, the

performance of the two models ~~seems~~ is generally comparable.
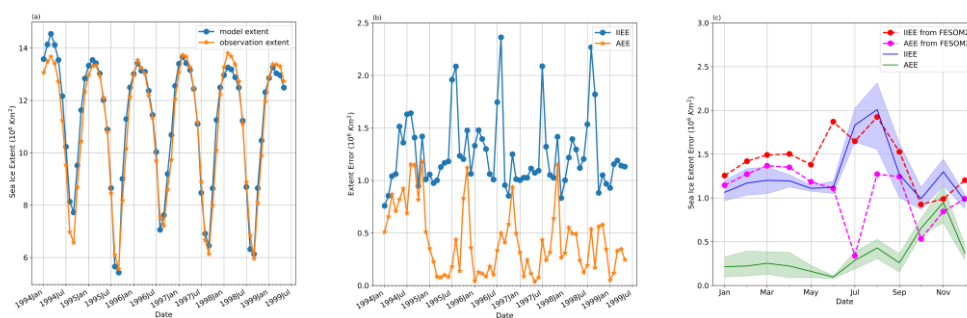
Figure ~~7~~8. (a) Monthly sea ice extent of model and observation in the Arctic Ocean. **(b)** Monthly Integrated Ice

505 Edge Error (IIEE) and Absolute Extent Error (AEE). **(c)** Monthly IIEE and AEE of SCHISM-Icepack ~~our model~~

and FESOM2 (averaged across all years), with the shading representing the 95% confidence intervals.

The comparison of the spatial sea ice concentration is shown in Fig.~~8~~9. The simulated sea ice boundary

and ice concentration show good agreement with satellite observations~~the observation~~, and the model

shows a robust ability to capture the seasonal evolution of sea ice in the Arctic Ocean. During winter

510 and spring (Fig. ~~8a~~9a and ~~8b~~9b), the deviation occurs in the marginal ice zone, such as the Bering Sea

and the Greenland Sea~~the Atlantic Ocean~~. In summer (Fig.~~8c~~9c), the model overestimates the sea ice concentration near the coast, such as the Canadian archipelago coast, but underestimates in the central Arctic Basin. The overestimation is likely due to the model's simplified representation of~~the presence of~~ complex thermodynamic and dynamic processes in the coastal margin (e.g., the occurrence of landfast sea ice). Furthermore, the lack of precise runoff and temperature data of Arctic rivers has a significant impact on the coastal area simulation. In the central Arctic Basin, melt ponds have a significant effect on the mass of sea ice during the melting season, and they are typically ~~always~~ formed as a certain amount of precipitation remains on the ice (Feng et al., 2022). The precipitation field we utilized shows ~~some~~ slightly overestimation compared to the observation-based precipitation products (Marcovecchio et al., 2021), so it is plausible that the underestimation of sea ice concentration in the central Arctic Basin is ~~likely due to~~caused by the excessive melt ponds that were reproduced in SCHISM-Icepack~~our model~~. In autumn (Fig.~~8d~~9d), the model overestimates sea ice concentration in the marginal seas of the Arctic, such as ~~like~~ Hudson and Baffin Bay, which causes the largest AEE. The heat exchange ~~between~~ at the air-ice-sea interface is generally more intense in the freezing season compared to the ~~than~~ melting season, so the coupled model may generate more sea ice due to its inability to deliver sufficient heat to the surface in time or due to the underrepresented ~~insufficient~~ strength of convection in the upper ocean.
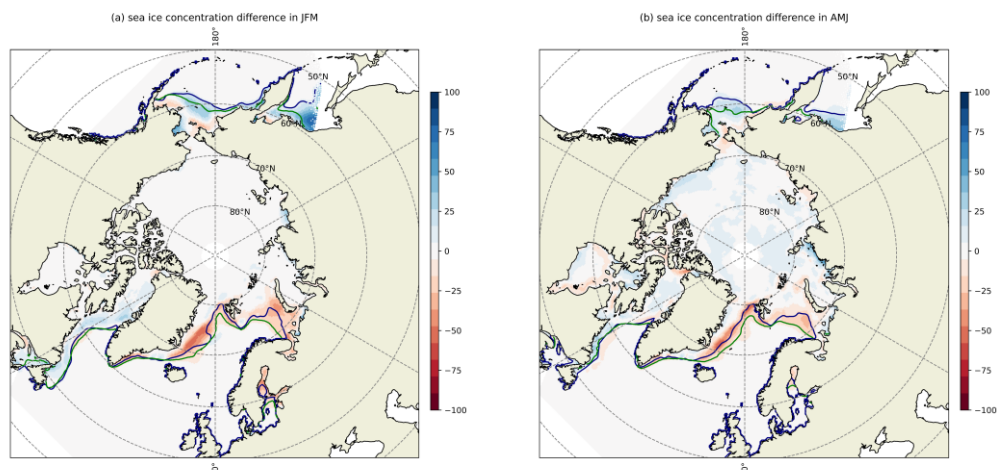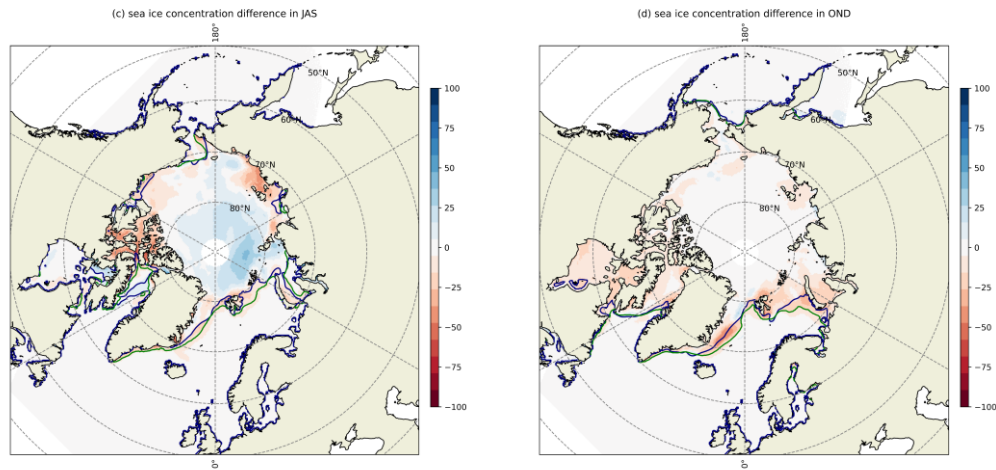
530 **Figure ~~8~~9.** Seasonally averaged sea ice concentration difference (Observation-Model). The blue line is the satellite sea ice boundary, and the green line is from the model. **(a)** Winter (Jan. Feb. and Mar.), **(b)** Spring (Apr. May. and Jun.), **(c)** Summer (Jul. Aug. and Sept.), **(d)** Autumn (Oct. Nov. and Dec.)

~~Another comparison of t~~The sea ice thickness is also validated ~~shown in Fig.10~~. The observed ice
535 thickness data, derived from upward-looking sonar sea ice draft measurements, were collected by submarines of the SCience ICe EXercise (SCICEX, National Snow and Ice Data Center, 1998). The in-situ data are compared with the corresponding model values using a box plot in Fig. 10. The ~~results of~~ model results ~~are close to~~closely match~~well match~~ the observations in Apr. 1994, Sept. 1997, Aug. ~~1998~~1998, and Apr. 1999, while the bias of the mean thickness is less than 0.6m~~, while~~. ~~lower~~
540 Underestimation of the ice thicknesses happens in other months, ~~and the underestimations~~with the bias of the mean thickness ranging from approximately 1.0m to 1.5~~being~~m. Specifically in the springs of 1994 and 1999 (April both years and May in 1999), the median thickness exhibits a bias of about 0.6m, which is smaller than over half of the individual CMIP5 models during the same season, where median thickness biases exceed 1.0m (Stroeve et al., 2014). Overall, SCHISM-Icepack demonstrates a robust capability to
545 replicate both the observed seasonal and interannual variability of sea ice thickness.
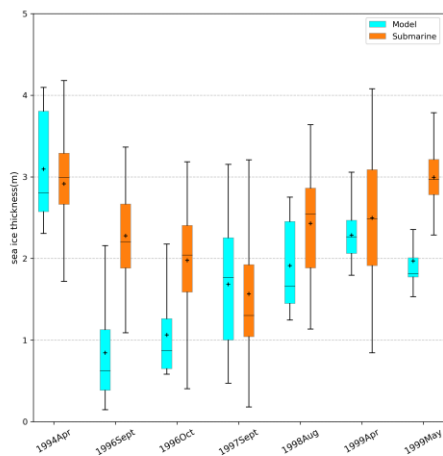
Figure 10. The box plot of sea ice thickness comparation. Cyan is the model result and orange is the data from submarine. In this study, the grid definition is different between the ice module and the hydrodynamic module. The ice module uses the Arakawa A grid, and all tracers and velocities are defined at nodes, while the hydrodynamic module uses the Arakawa CD grid. The main reason behind this decision is that we adapted the rheology part from FESIM, which uses an analogue of the Arakawa A grid, and it performs well for sea ice simulation while saving computational costs (Danilov et al., 2015). For a coarse mesh, the Arakawa A grid delivers performance similar to that of the Arakawa CD grid in simulating sea ice deformations (Mehlmann et al., 2021). In a pure advection case, the oscillations are weaker for the Arakawa A grid with tracers located at the node, compared to the case with the tracers located at the centroid (Zhang et al., 2016). The coupling between the ice module and the hydrodynamic module remains unaffected by the differences in the variable definition, as all forcing variables are located at nodes in the hydrodynamic module. Under the uniform mesh in the idealized test, the central difference scheme is similar to the second order upstream scheme of UG-CICE, and the latter achieved remarkable results (Gao et al., 2013). The difference in stencils used between UG-CICE and this work may explain why the central difference scheme has an unsatisfactory performance: in UG-CICE, tracers are also at vertices (nodes) but the velocity is at the centroids. Still, it remains unclear if UG-CICE is strictly monotone.

The TVD scheme used in this work is based on the gradient of the central node, whereas Casulli et al. (2005) used the flux into the element to obtain the ϕ_{U*} in order to avoid unphysical overshoots/undershoots. For the Casulli's TVD scheme, the tracers are always located at the centroid,

but they also can be converted to the node (Zhang et al., 2016). A comparison of the results for the idealized cases from Casulli's TVD and our TVD scheme revealed that Casulli's TVD scheme has more diffusion than the new TVD scheme.

5 4 Conclusion

We have incorporated a multi-class sea ice module, the advanced sea ice column physics package Icepack, into the SCHISM modelling system. Significantly, we have implemented a new TVD based scheme for ice tracer transport and validated it using through an idealized case and realistic cases. The simulation results reveal demonstrate that the TVD scheme is conservative, accurate, strictly monotonic, and efficient in reproducing the horizontal transport of ice, and has better performance than the second-order upwind scheme. Particularly, it provides strict monotonicity, which is crucial for stability, thus addressinges the difficulties encountered in the single-class ice model utilizing the FEM-FCT. and has better performance than the upwind and central schemes. The coupled SCHISM-Icepack model improves the results of the previous single-class ice model in the case of the Lake Superior, and for the Arctic Ocean was able to reproduce the Arctic Sea ice concentration, boundary, and extent and thickness as seen from the observation.

An advantage of the coupled model SCHISM-Icepack is its ability to effectively simulate the sophisticated ocean-ice evolution in both open ocean and coastal regions. In addition,regions. SCHISM includes various biogeochemistry modules like CoSiNE, while Icepack provides more detailed insights into the evolution of sea ice andIcepack contains a biogeochemical stry module as wellprocesses. By integrating these biogeochemistry and physical modules in future work, we can deepen our investigation into the changes within under-ice ecosystems resulting from global warming. We will further investigate the under-ice ecosystem changes caused by global warming by integrating those biogeochemistry modules.

Code and data availability.

595 Code of this model have two components, Icepack 1.3.4 and SCHISM v5.11. Icepack 1.3.4 is obtained from https://github.com/CICE-Consortium/Icepack . SCHISM v5.11 and the coupled model can be found at https://github.com/schism-dev/schism, including all the code used in this paper. All source code is also available on Zenodo (https://doi.org/10.5281/zenodo.10391035, Wang et al., 2023) with all configuration files of the idealized case and the realistic test on the Arctic Ocean. In the realistic test on

600 the Arctic Ocean, the forcing data is from ERA5, initial and boundary data is from HYCOM and FES2014, they can be generated by the preprocessing script in SCHISM. The input data of the realistic case on the Lake Superior is available from Y. Joseph Zhang on reasonable request. All the results in the paper are also available from Qian Wang on reasonable request.

605 **Author contributions**

Qian Wang: Data curation, Formal analysis, Investigation, Methodology, Software, Visualization, Writing – original draft preparation. ~~Fei Chai: Conceptualization, Supervision, Funding acquisition, Project administration.~~ **Yang Zhang**: Validation, Resources, Software, Writing – review & editing. **Fei Chai**: Conceptualization, Supervision, Funding acquisition, Project administration. **Y. Joseph Zhang**:

610 Validation, Methodology, Software, Writing – review & editing. **Lorenzo Zampieri ~~Zamperi~~**: Writing – review & editing.

Competing interests

The authors declare that they have no conflict of interest.

Acknowledgements

615 The authors acknowledge the financial support of the National Natural Science Foundation of China (Grant Number 41941013). The study in this paper was supported by the high-performance computing clusters at: (1) State Key Laboratory of Satellite Ocean Environment Dynamics, SIO, MNR; (2) William & Mary Research Computing (URL: https://www.wm.edu/it/rc). The authors also thank HYCOM data server for their sea ice product. Lorenzo Zampieri acknowledges the financial support of the Italian

620 National Recovery and Resilience Plan (PNRR) through the "SPOKE 4 - EARTH & CLIMATE" program.

Financial support

This work is supported by the National Natural Science Foundation of China (Grant Number 41941013)

625 **References**

Alistair Adcroft, Jean-Michel Campin, Ed Doddridge, Stephanie Dutkiewicz, Constantinos Evangelinos, David Ferreira, Mick Follows, Gael Forget, Baylor Fox-Kemper, Patrick Heimbach, Chris Hill, Ed Hill, Helen Hill, Oliver Jahn, Jody Klymak, Martin Losch, John Marshall, Guillaume Maze, Matt Mazloff, Dimitris Menemenlis, Andrea Molod, and Jeff Scott. MITgcm user manual. Massachusetts Institute of

630 Technology, https://readthedocs.org/projects/mitgcm/downloads/pdf/latest/, 2023.

Bitz, C. M., Holland, M. M., Weaver, A. J., & Eby, M. Simulating the ice-thickness distribution in a coupled climate model. Journal of Geophysical Research: Oceans, 106(C2), 2441-2463, https://doi.org/10.1029/1999JC000113, 2001.

Bitz, C. M. and Lipscomb, W. H.: An energy-conserving thermodynamic model of sea ice, J. Geophys.

635 Res.-Oceans, 104, 15669–15677, https://doi.org/10.1029/1999JC900100, 1999.

Briegleb, B. P. and Light, B.: A Delta-Eddington multiple scattering parameterization for solar radiation in the sea ice component of the Community Climate System Model, Tech. Rep. NCAR/TN 472+STR, National Center for Atmospheric Research, Boulder, Colorado USA, https://doi.org/10.5065/D6B27S71, 2007.

640 Budgell, W. P., Oliveira, A., and Skogen, M. D.: Scalar advection schemes for ocean modelling on unstructured triangular grids, Ocean Dynamics, 57, 339-361, https://doi.org/10.1007/s10236-007-0111-8, 2007.

Casulli, V. and Zanolli, P.: High resolution methods for multidimensional advection–diffusion problems in free-surface hydrodynamics, Ocean Modelling, 10, 137-151,

645 https://doi.org/10.1016/j.ocemod.2004.06.007, 2005.

Chen, C., Beardsley, R. C., Cowles, G., Qi, J., Lai, Z., Gao, G., ... & Lin, H. An unstructured-grid, finite-volume community ocean model: FVCOM user manual. Cambridge, MA, USA: Sea Grant College Program, Massachusetts Institute of Technology. 2012.

Danilov, S., Sidorenko, D., Wang, Q., and Jung, T.: The Finite-volumE Sea ice–Ocean Model (FESOM2),

650 Geoscientific Model Development, 10, 765-789, https://doi.org/10.5194/gmd-10-765-2017, 2017.

Danilov, S., Wang, Q., Timmermann, R., Iakovlev, N., Sidorenko, D., Kimmritz, M., Jung, T., and Schröter, J.: Finite-Element Sea Ice Model (FESIM), version 2, Geoscientific Model Development, 8, 1747-1761, https://doi.org/10.5194/gmd-8-1747-2015, 2015.

655 ~~Darwish, M. S., & Moukalled, F. TVD schemes for unstructured grids. International Journal of heat and mass transfer, 46(4), 599-611. https://doi.org/10.1016/S0017-9310(02)00330-7, 2003.~~

Elizabeth Hunke, Richard Allard, David A. Bailey, Philippe Blain, Anthony Craig, Frederic Dupont, Alice DuVivier, Robert Grumbine, David Hebert, Marika Holland, Nicole Jeffery, Jean-Francois Lemieux, Robert Osinski, Till Rasmussen, Mads Ribergaard, Lettie Roach, Andrew Roberts, Matthew Turner, & Michael Winton. CICE-Consortium/Icepack: Icepack 1.3.4 (1.3.4). Zenodo.

660 https://doi.org/10.5281/zenodo.8336034, 2023.

Feng, J., Zhang, Y., Cheng, Q., and Tsou, J. Y.: Pan-Arctic melt pond fraction trend, variability, and contribution to sea ice changes, Global and Planetary Change, 217, https://doi.org/10.1016/j.gloplacha.2022.103932, 2022.

Fetterer, F., K. Knowles, W. N. Meier, M. Savoie, and A. K. Windnagel.. Sea Ice Index, Version 3 [Data

665 Set]. Boulder, Colorado USA. National Snow and Ice Data Center. https://doi.org/10.7265/N5K072F8. Date Accessed 08-05-2023. 2017.

Gao, G., Chen, C., Qi, J., and Beardsley, R. C.: An unstructured-grid, finite-volume sea ice model: Development, validation, and application, Journal of Geophysical Research, 116, https://doi.org/10.1029/2010JC006688, 2011.

670

Goessling, H. F., Tietsche, S., Day, J. J., Hawkins, E., and Jung, T.: Predictability of the Arctic sea ice edge, Geophysical Research Letters, 43, 1642-1650, https://doi.org/10.1002/2015GL067232, 2016.

Great Lakes Surface Environmental Analysis (GLSEA): https://coastwatch.glerl.noaa.gov/satellite-data-products/great-lakes-surface-environmental-analysis-glsea/, , last access: 2 April 2024.

675 Hersbach, H., Bell, B., Berrisford, P., Hirahara, S., Horányi, A., Muñoz-Sabater, J., ... & Thépaut, J. N. The ERA5 global reanalysis. Quarterly Journal of the Royal Meteorological Society, 146(730), 1999-2049. https://doi.org/10.1002/qj.3803, 2020.

Hunke, E. C. Thickness sensitivities in the CICE sea ice model. Ocean Modelling, 34(3-4), 137-149. https://doi.org/10.1016/j.ocemod.2010.05.004, 2010.

680 Hunke, E., Allard, R., Blain, P., Blockley, E., Feltham, D., Fichefet, T., Garric, G., Grumbine, R., Lemieux, J. F., Rasmussen, T., Ribergaard, M., Roberts, A., Schweiger, A., Tietsche, S., Tremblay, B., Vancoppenolle, M., and Zhang, J.: Should Sea-Ice Modeling Tools Designed for Climate Research Be Used for Short-Term Forecasting?, Curr Clim Change Rep, 6, 121-136, https://doi.org/10.1007/s40641-020-00162-y, 2020.

685 Hunke, E. C. and Dukowicz, J. K.: An elasticviscous-plastic model for sea ice dynamics, J. Phys. Oceanogr., 27, 1849–1867, https://doi.org/10.1175/1520-0485(1997)027<1849:AEVPMF>2.0.CO;2, 1997.

Hunke, E. C., Hebert, D. A., & Lecomte, O. Level-ice melt ponds in the Los Alamos sea ice model, CICE. Ocean Modelling, 71, 26-42. https://doi.org/10.1016/j.ocemod.2012.11.008, 2013

690 ~~–~~Hunke, E. C., Lipscomb, W. H., Turner, A. K., Jeffery, N., and Elliott, S.: CICE: the Los Alamos sea ice model documentation and software user's manual version 5.1, Tech. Rep., Los Alamos National Laboratory, LA-CC-06-012, https://github.com/CICE-Consortium/CICE-svn-trunk/blob/main/cicedoc/cicedoc.pdf (last access: 4 April 2022), 2015.

Hunke, E. C., Lipscomb, W. H., & Turner, A. K. Sea-ice models for climate study: retrospective and new 695 directions. Journal of Glaciology, 56(200), 1162-1172. https://doi.org/10.3189/002214311796406095, 2010.

Hurrell, J. W., Holland, M. M., Gent, P. R., Ghan, S., Kay, J. E., Kushner, P. J., ... & Marshall, S. The community earth system model: a framework for collaborative research. Bulletin of the American Meteorological Society, 94(9), 1339-1360. https://doi.org/10.1175/BAMS-D-12-00121.1, 2013.

700 ~~Jean Michel Campin, Patrick Heimbach, Martin Losch, Gael Forget, edhill3, Alistair Adcroft, amolod, Dimitris Menemenlis, dfer22, Oliver Jahn, Chris Hill, Jeff Scott, stephdut, Matt Mazloff, Baylor Fox-Kemper, antnguyen13, Ed Doddridge, Ian Fenty, Michael Bates, Timothy Smith, AndrewEichmann-NOAA, mitllheisey, Jonathan Lauderdale, Torge Martin, Ryan Abernathey, Ou Wang, samarkhatiwala, dngoldberg, hongandyanand Bruno Deremble: MITgcm/MITgcm: ckeckpoint68r, 705 https://doi.org/10.5281/zenodo.8208482, 2 August 2023.~~

Kimmritz, M., Danilov, S., and Losch, M.: On the convergence of the modified elastic-viscous-plastic method for solving the sea ice momentum equation, J. Comput. Phys., 296, 90–100, https://doi.org/10.1016/j.jcp.2015.04.051, 2015.~~Lipscomb, W. H. Remapping the thickness distribution in sea ice models, J. Geophys. Res., 106(C7), 13989–14000, doi:10.1029/2000JC000518, 2001.~~

710

Lipscomb, W. H. Remapping the thickness distribution in sea ice models, *J. Geophys. Res.*, 106(C7), 13989–14000, doi:10.1029/2000JC000518, 2001.

Lipscomb, W. H. and Hunke, E. C.: Modeling sea ice transport using incremental remapping, Mon.

715 Weather Rev., 132, 1341–1354, https://doi.org/10.1175/1520-0493(2004)132<1341:MSITUI>2.0.CO;2, 2004.

Lipscomb, W. H., Hunke, E. C., Maslowski, W., and Jakacki, J.: Ridging, strength, and stability in high-resolution sea ice models, Journal of Geophysical Research: Oceans, 112, https://doi.org/10.1029/2005JC003355, 2007.

720 Löhner, R., Morgan, K., Peraire, J., & Vahdati, M. Finite element flux-corrected transport (FEM–FCT) for the euler and Navier–Stokes equations. International Journal for Numerical Methods in Fluids, 7(10), 1093-1109. https://doi.org/10.1002/fld.1650071007, 1987.

Lyard, F. H., Allain, D. J., Cancet, M., Carrère, L., & Picot, N.. FES2014 global ocean tide atlas: design and performance. Ocean Science, 17(3), 615-649. https://doi.org/10.5194/os-17-615-2021, 2021.

725 Madec Gurvan, Romain Bourdallé-Badie, Jérôme Chanut, Emanuela Clementi, Andrew Coward, Christian Ethé, Doroteaciro Iovino, Dan Lea, Claire Lévy, Tomas Lovato, Nicolas Martin, Sébastien Masson, Silvia Mocavero, Clément Rousset, Dave Storkey, Simon Müeller, George Nurser, Mike Bell, Guillaume Samson, Pierre Mathiot, Francesca Meleand Aimie Moulin: NEMO ocean engine, https://doi.org/10.5281/zenodo.6334656, 7 March 2022.

730 Marcovecchio, A., Behrangi, A., Dong, X., Xi, B., and Huang, Y.: Precipitation influence on and response to early and late Arctic sea ice melt onset during melt season, International Journal of Climatology, 42, 81-96, https://doi.org/10.1002/joc.7233, 2021.

M.S. Darwish, F. Moukalled. TVD schemes for unstructured grids. International Journal of Heat and Mass Transfer, 46(4), 599-611. https://doi.org/10.1016/S0017-9310(02)00330-7, 2003.

735 Mehlmann, C., Danilov, S., Losch, M., Lemieux, J. F., Hutter, N., Richter, T., Blain, P., Hunke, E. C., and Korn, P.: Simulating Linear Kinematic Features in Viscous-Plastic Sea Ice Models on Quadrilateral and Triangular Grids With Different Variable Staggering, Journal of Advances in Modeling Earth Systems, 13, https://doi.org/10.1029/2021MS002523, 2021.

740 ~~Meredith, M., Sommerkorn, M., Cassota, S., Derksen, C., Ekaykin, A., Hollowed, A., Kofinas, G., Mackintosh, A., Melbourne Thomas, J., Muelbert, M., Ottersen, G., Pritchard, H., Schuur, E., Boyd, P., Hobbs, W. and Hodgson-Johnston, I.: Polar Regions, https://hdl.handle.net/102.100.100/516805, 2019.~~National Snow and Ice Data Center (comp.). Submarine Upward Looking Sonar Ice Draft Profile Data and Statistics, Version 1 [Data Set]. Boulder, Colorado USA. National Snow and Ice Data Center. https://doi.org/10.7265/N54Q7RWK. Date Accessed 03-23-2024. 1998.

745 Parkinson, C. L. and Washington, W. M.: A large-scale numerical model of sea ice, J. Geophys. Res., 84, 311–337, https://doi.org/10.1029/JC084iC01p00311, 1979.

Rothrock, D. A.: The energetics of the plastic deformation of pack ice by ridging, Journal of Geophysical Research, 80, 4514-4519, https://doi.org/10.1029/JC080i033p04514, 1975.

Stroeve, J., Barrett, A., Serreze, M., and Schweiger, A.: Using records from submarine, aircraft and 750 satellites to evaluate climate model simulations of Arctic sea ice thickness, The Cryosphere, 8, 1839–1854, https://doi.org/10.5194/tc-8-1839-2014, 2014.

Sweby, P. K. High resolution schemes using flux limiters for hyperbolic conservation laws. SIAM journal on numerical analysis, 21(5), 995-1011. https://doi.org/10.1137/0721062, 1984.

Thorndike, A. S., Rothrock, D. A., Maykut, G. A., and Colony, R., The thickness distribution of sea ice, 755 J. Geophys. Res., 80(33), 4501–4513, https://doi.org/10.1029/JC080i033p04501, 1975.

The U.S. National Ice Center (USNIC) : https://usicecenter.gov/ last access: 2 April 2024.

Turner, A. K., Hunke, E. C., and Bitz, C. M.: Two modes of sea-ice gravity drainage: A parameterization for largescale modeling, J. Geophys. Res.-Oceans, 118, 2279–2294, https://doi.org/10.1002/jgrc.20171, 2013.

760 Turner, A. K., Lipscomb, W. H., Hunke, E. C., Jacobsen, D. W., Jeffery, N., Engwirda, D., Ringler, T. D., and Wolfe, J. D.: MPAS-Seaice (v1.0.0): sea-ice dynamics on unstructured Voronoi meshes, Geoscientific Model Development, 15, 3721-3751, https://doi.org/10.5194/gmd-15-3721-2022, 2022.

Umlauf, L., & Burchard, H. A generic length-scale equation for geophysical turbulence models. Journal of Marine Research, 61(2), 235-265. http://dx.doi.org/10.1357/002224003322005087 2003.

765 Van Leer, B. Towards the ultimate conservative difference scheme. V. A second-order sequel to Godunov's method. Journal of computational Physics, 32(1), 101-136. https://doi.org/10.1016/0021-9991(79)90145-1, 1979.

Wang, Q., Chai, F., Zhang, Y., Zhang, J. Y., & Zampieri Zamperi, L. Dataset of 'Development of a total variation diminishing (TVD) Sea ice transport scheme and its application in in an ocean (SCHISM v5.11) and sea ice (Icepack v1.3.4) coupled model on unstructured grids' [Data set]. Zenodo. https://doi.org/10.5281/zenodo.10391035, 2023.

Ye F, Zhang Y, Friedrichs M, Wang HV, Irby I, Shen J, Wang Z., A 3D, cross-scale, baroclinic model with implicit vertical transport for the Upper Chesapeake Bay and its tributaries. Ocean Model 107:82–96. https://doi.org/10.1016/j.ocemod.2016.10.004,2016.

Zampieri, L., Goessling, H. F., & Jung, T. Bright Prospects for Arctic Sea Ice Prediction on Subseasonal Time Scales. In Geophysical Research Letters (Vol. 45, Issue 18, pp. 9731–9738). https://doi.org/10.1029/2018gl079394, 2018

Zampieri, L., Kauker, F., Fröhle, J., Sumata, H., Hunke, E. C., and Goessling, H. F.: Impact of Sea-Ice Model Complexity on the Performance of an Unstructured-Mesh Sea-Ice/Ocean Model under Different Atmospheric Forcings, Journal of Advances in Modeling Earth Systems, 13, https://doi.org/10.1029/2020MS002438, 2021.

Zeng, X., Zhao, M., & Dickinson, R. E. Intercomparison of bulk aerodynamic algorithms for the computation of sea surface fluxes using TOGA COARE and TAO data. Journal of Climate, 11(10), 2628-2644. https://doi.org/10.1175/1520-0442(1998)011%3C2628:IOBAAF%3E2.0.CO;2, 1998.

Zhang, D., Jiang, C., Liang, D., and Cheng, L.: A review on TVD schemes and a refined flux-limiter for steady-state calculations, Journal of Computational Physics, 302, 114-154, https://doi.org/10.1016/j.jcp.2015.08.042, 2015.

Zhang, Y. and Baptista, A.M. SELFE: A semi-implicit Eulerian-Lagrangian finite-element model for cross-scale ocean circulation", Ocean Modelling, 21(3-4), 71-96. https://doi.org/10.1016/j.ocemod.2007.11.005, 2008.

Zhang, Y. J., Ateljevich, E., Yu, H. C., Wu, C. H., & Jason, C. S. A new vertical coordinate system for a 3D unstructured-grid model. Ocean Modelling, 85, 16-31. https://doi.org/10.1016/j.ocemod.2014.10.003, 2015.

Zhang, Y. J., Ye, F., Stanev, E. V., and Grashorn, S.: Seamless cross-scale modeling with SCHISM, Ocean Modelling, 102, 64-81, https://doi.org/10.1016/j.ocemod.2016.05.002, 2016.

Zhang, Y. J., Wu, C., Anderson, J., Danilov, S., Wang, Q., Liu, Y., and Wang, Q.: Lake ice simulation using a 3D unstructured grid model, Ocean Dynamics, 73, 219-230, https://doi.org/10.1007/s10236-023-01549-9, 2023.

800 ~~Zhang, Z., Song, Z.-y., Guo, F., Zhang, D., Wen, Y.-n., and Hu, D.: Comparison and modification: TVD schemes for scalar transport on an unstructured grid, China Ocean Engineering, 30, 615-626, https://doi.org/10.1007/s13344-016-0039-1, 2016.~~

Zhang, Z., Song, Z.-y., Kong, J., and Hu, D.: A new r-ratio formulation for TVD schemes for vertex-centered FVM on an unstructured mesh, International Journal for Numerical Methods in Fluids, 81, 741-764, https://doi.org/10.1002/fld.4206, 2016.

805